Available online at www.sciencedirect.com

ScienceDirect

Mendeleev Commun., 2023, **33**, 861–863

Mendeleev Communications

Ni^{II} and Cu^{II} coordination polymers as anode materials and their compatibility with different electrolytes in Li-ion batteries

Guzaliya R. Baymuratova,*[a] Ekaterina A. Komissarova,[a] Galiya Z. Tulibaeva,[a] Olga V. Yarmolenko,[a] Olga A. Kraevaya[a] and Pavel A. Troshin[a,b,c]

[a] *Federal Research Center of Problems of Chemical Physics and Medicinal Chemistry, Russian Academy of Sciences, 142432 Chernogolovka, Moscow Region, Russian Federation. E-mail: guzalia.rb@yandex.ru*
[b] *Zhengzhou Research Institute, Harbin Institute of Technology, 450003 Zhengzhou, China*
[c] *Harbin Institute of Technology, 150001 Harbin, China*

DOI: 10.1016/j.mencom.2023.10.041

The effect of various types of electrolytes on the operation of coordination polymers based on Ni^{II} or Cu^{II} in lithium-ion batteries has been examined. Cyclic voltammetry, galvanostatic cycling and quantum chemical modeling have been used to study the processes of lithiation and delithiation. It was shown that the use of a new electrolyte based on a mixture of 1 M $LiN(CF_3SO_2)_2$ in 1,3-dioxolane–1,2-dimethoxyethane and 1 M $LiPF_6$ in ethylene carbonate–dimethyl carbonate improved battery performance, while cycling in the range of 0.2–2.5 V increased the discharge capacity up to 177–188 mA h g^{-1} and stabilized the charge–discharge processes.

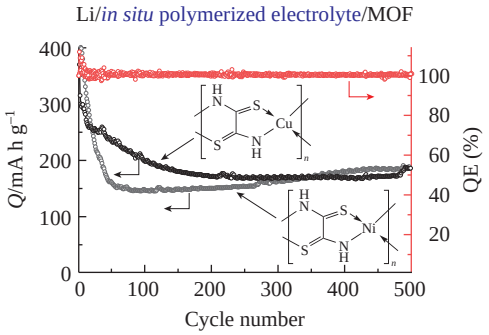

Keywords: MOF, lithium battery, discharge capacity, *in situ* polymerized electrolyte, $LiPF_6$, dioxolane.

Currently, materials based on metal–organic frameworks (MOFs) are of particular interest.[1–4] Promising redox-active materials with high electronic conductivity (1 S cm^{-1}) and controlled electrochemical properties are *d*–π conjugated coordination polymers synthesized from arylamines/thiophenols and Ni^{II} or Cu^{II} salts.[5–9] The development of new safe electrolyte systems for lithium ion batteries (LIBs) is also an important task.[10–15] The low stability of pure MOFs and composites based on them has to be overcome, and there are also limitations due to electrolyte decomposition potentials.

In the previous work,[15] we obtained coordination polymers, nickel rubeanate **P1** and copper rubeanate **P2** (Scheme S1, see Online Supplementary Materials).

The electronic conductivity of complexes **P1** and **P2** was measured (Figure S1, see Online Supplementary Materials). At 21 °C, the electrical conductivity (σ) of the nickel- and copper-based complexes was 0.19 and 0.17 S cm^{-1}, respectively. These values are lower than those of metal complexes with hexaaminobenzene (10 S cm^{-1} at 27 °C).[16]

The average particle size of the complex **P1** powder is 19.73 μm, and the particle diameter ranges from 0.8 to 62 μm [Figure S2(*a*)]. For complex **P2**, the average particle size is 17.33 μm, and the particle sizes are in the range of 0.6–43 μm [Figure S2(*b*)].

Scheme 1 shows the proposed charge–discharge mechanism involving 2 ē and 2 Li^+. In the case of these transformations, the theoretical capacity of complexes **P1** and **P2** is 303 and 295 mA h g^{-1}, respectively.

To understand the difference between redox transformations, quantum chemical modeling of complexes **P1** and **P2** was carried out. All calculations were carried out by the density functional method using the Priroda[17] software package. The quantum chemical calculation method is described in detail in Online Supplementary Materials.

In the case of nickel, the polymer chain has a planar structure [Figure S3(*a*)], in contrast to the polymer with copper [Figure S3(*b*)], where the chains twist along their axis. Several isomeric structures with different positions of lithium atoms (Li_{20}) relative to the polymer plane were found (Figure 1).

First, we searched for a suitable electrolyte system for the studied MOFs. We used three different electrolytes. Electrolyte no. 1 consisted of 1 M $LiN(CF_3SO_2)_2$ (LiTFSI) in 1,3-dioxolane–1,2-dimethoxyethane (DOL–DME, 2 : 1, v/v). Electrolyte no. 2 was 1 M LiTFSI in tetraglyme. Electrolyte system no. 3 was prepared from a mixture of 1 M LiTFSI in DOL–DME and 1 M $LiPF_6$ in ethylene carbonate–dimethyl carbonate (EC–DMC, 1 : 1, v/v) by *in situ* polymerization of dioxolane induced by $LiPF_6$.[14]

To study the electrode/electrolyte interface by the method of electrochemical impedance, symmetrical cells **P1**//**P1** and **P2**//**P2** were assembled for each of the three electrolytes. Figure S4 shows Nyquist plots and equivalent circuit models. Table S1 shows the calculated parameters of the equivalent cell circuits. It can be seen that the minimum resistance *W*1–*R* at the electrode/electrolyte interface is demonstrated by cells with electrolyte no. 3.

Analysis of Li//**P1**(**P2**) cells by cyclic voltammetry (CV) was carried out in the range of 0.5–3.0 V at a scan rate of 1 mV s^{-1} (Figure S5). For the Li//**P1** cell with electrolyte no. 1, the most pronounced peaks are observed in the 1st cycle, and each subsequent

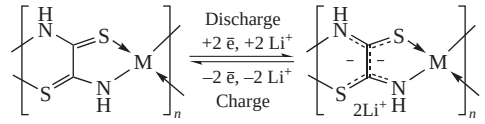

P1 M = Ni, **P2** M = Cu

Scheme 1 Redox transformations of MOFs.

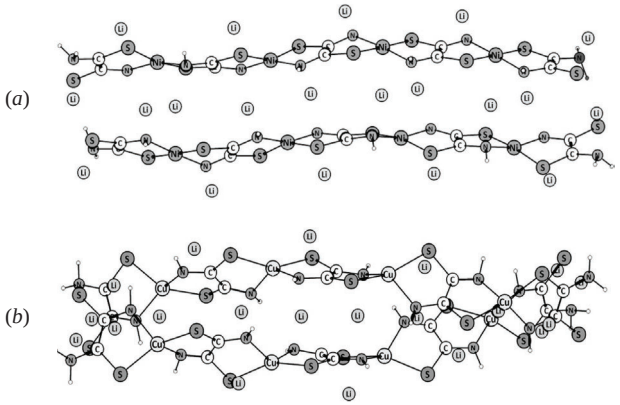

Figure 1 Quantum chemical models of (*a*) $(\mathbf{P1})_2Li_{20}$ and (*b*) $(\mathbf{P2})_2Li_{20}$.

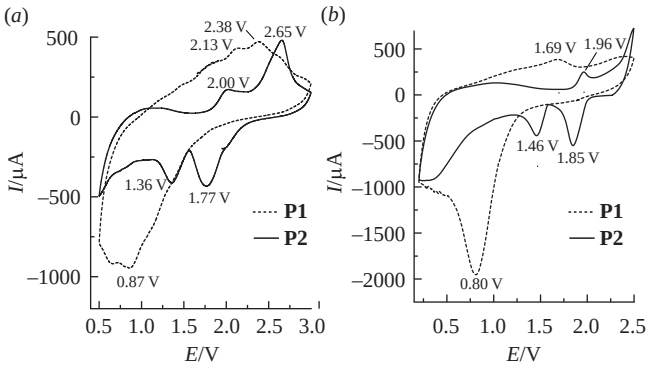

Figure 3 CV curves of Li//**P1** and Li//**P2** cells with electrolyte no. 3 in the voltage ranges of (*a*) 0.5–3.0 and (*b*) 0.2–2.5 V at a scan rate of 1 mV s^{-1}.

cycle shifts to the right, which probably indicates a structural modification of the active material [Figure S5(*a*)]. A significant difference between the CV curves of Li//**P2** in different electrolytes is observed in the cathode region, demonstrating a double peak at 1.88 and 2.05 V for electrolyte no. 1 and single peaks at 1.95 and 2.02 V for electrolytes no. 2 and no. 3, respectively.

Charge–discharge tests of Li//**P1**(**P2**) cells were carried out in the voltage range of 0.5–3.0 V with three electrolytes at a current density of 0.15 A g^{-1} (Figure S6). It is shown that for cells with electrolyte no. 3, the discharge capacity is higher during the first 120 cycles than for cells with electrolytes no. 1 and no. 2. The electrochemical behavior of Li//**P1** and Li//**P2** cells at the initial stage is different, but after 50 charge–discharge cycles, their capacities are the same and amount to ~102 mA h g^{-1} (Figure 2).

In the first part of the work, it was shown that the use of an *in situ* polymerized mixture of two electrolytes (electrolyte no. 3) is promising for this electrochemical system, since this leads to an increase in the discharge capacity of the material and a decrease in the resistance at the electrode/electrolyte interface.

In further studies, the optimal voltage range of 0.2–2.5 V was selected for Li//**P1**(**P2**) cells with the *in situ* polymerized electrolyte (electrolyte no. 3).

In this voltage range, the CV peaks in the cathode (1.7 V) and anode (0.8 V) regions are more pronounced than in the range of 0.5–3.0 V, which indicates a decrease in diffusion difficulties (Figure 3). Changing the potential window for the Li//**P2** cell did not affect the number of peaks in the anode regions (1.46 and 1.85 V), but was accompanied by their shift to the right. In the cathode region, one peak remained at ~2 V with no offset. Each polymer unit in the MOF can theoretically undergo two-electron reduction by accepting two lithium ions (see Scheme S1). In the first CV cycle, two peaks are observed in both the anodic and cathodic regions, which are responsible for the redox transition of the MOF functional groups. So for Li//**P2** [Figure 3(*b*)] the first reduction and oxidation involving one lithium ion occurs at 1.85 and 2.5 V, respectively. The second redox transition occurs at 1.46 and 1.96 V, respectively. The broad peak at 0.8 V corresponds to the intercalation of lithium into the carbon material.

The charge–discharge profiles for the Li//**P1** cell are completely reversible in the 1st cycle, and for the Li//**P2** cell, the irreversible capacity in the 1st cycle is 37 mA h g^{-1}, which may be due to the formation of new phases at the interfaces between the electrolyte and electrodes and the incompleteness of the electrochemical reaction [Figure 4(*a*),(*b*)]. The loss of discharge capacity in the 1st and 10th cycles is 26–29% for Li//**P1**(**P2**). This may be due to both the dissolution of the electrode material and the irreversible lithiation of the electrode.

Galvanostatic cycling of the Li//**P1** cell showed that the discharge capacity in the 1st cycle is 450 mA h g^{-1}, and after 30 cycles it remains almost stable at 188 mA h g^{-1} [Figure 2(*c*)]. The discharge capacity of the Li//**P2** cell in the 3rd cycle is 310 mA h g^{-1}, and in

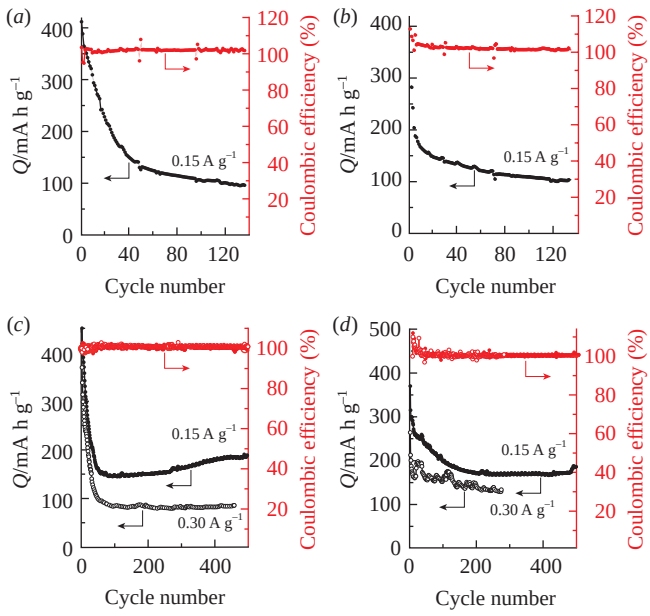

Figure 2 Dependence of the specific capacity and Coulombic efficiency of (*a*),(*c*) Li//**P1** and (*b*),(*d*) Li//**P2** cells on the number of cycles during galvanostatic cycling at a current density of 0.15 (solid circles) and 0.30 A g^{-1} (empty circles) in the voltage range of (*a*),(*b*) 0.5–3.0 and (*c*),(*d*) 0.2–2.5 V.

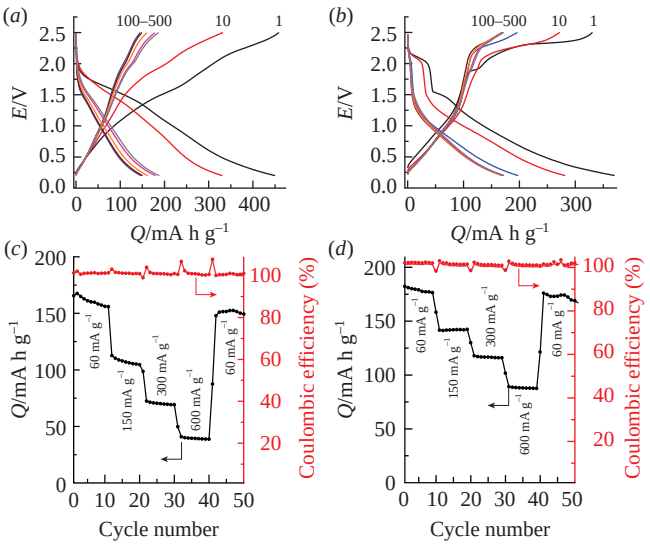

Figure 4 Charge–discharge profiles of the (*a*) Li//**P1** and (*b*) Li//**P2** cells in the voltage range of 0.2–2.5 V at a current density of 150 mA g^{-1}. Dependence of the specific capacity and Coulombic efficiency of the (*c*) Li//**P1** and (*d*) Li//**P2** cells on the current density.

the 500th cycle it is 172 mA h g^{-1} [Figure 2(*d*)]. The use of this electrolyte eliminates the solubility of organic cathodes during cycling, unlike liquid organic electrolytes (Figure S6).

Cell cycling at different current densities showed that electrode materials with the *in situ* polymerized electrolyte are able to recover well in the range of 0.2–2.5 V [Figure 4(*c*),(*d*)].

Thus, the electrolyte based on a mixture of 1 M LiTFSI in DOL–DME and 1 M $LiPF_6$ in EC–DMC showed the minimal resistance at the MOF/electrolyte interface. Furthermore, the capacitive performance of MOF-based electrodes when tested in lithium cells with the *in situ* polymerized electrolyte was higher than those in gel and ether electrolytes. The cycling of LIB with MOF electrodes and the polymerized electrolyte in the range of 0.2–2.5 V provides a high discharge capacity and stabilizes charge–discharge processes.

This work was supported by the Ministry of Science and Higher Education of the Russian Federation within the framework of the project ‘Laboratory of perspective electrode materials for chemical power sources’ [project no. FFSG-2022-0001 (1221117 00046-3)]. All quantum chemical calculations were carried out using the computational facilities of the Joint Supercomputer Center of the Russian Academy of Sciences.

Online Supplementary Materials

Supplementary data associated with this article can be found in the online version at doi: 10.1016/j.mencom.2023.10.041.

References

1 Y. Jiang, H. Zhao, L. Yue, J. Liang, T. Li, Q. Liu, Y. Luo, X. Kong, S. Lu, X. Shi, K. Zhou and X. Sun, *Electrochem. Commun.*, 2021, **122**, 106881.
2 T. Qiu, Z. Liang, W. Guo, H. Tabassum, S. Gao and R. Zou, *ACS Energy Lett.*, 2020, **5**, 520.
3 L. Feng, J.-L. Li, G. S. Day, X.-L. Lv and H.-C. Zhou, *Chem*, 2019, **5**, 1265.
4 R. Zhao, Z. Liang, R. Zou and Q. Xu, *Joule*, 2018, **2**, 2235.
5 R. R. Kapaev, S. Olthof, I. S. Zhidkov, E. Z. Kurmaev, K. J. Stevenson, K. Meerholz and P. A. Troshin, *Chem. Mater.*, 2019, **31**, 5197.
6 D. Wang, W. Hu, W. Fan, X. Xia, J. Liu and H. Liu, *Microporous Mesoporous Mater.*, 2021, **323**, 111240.
7 J. Xie, X.-F. Cheng, X. Cao, J.-H. He, W. Guo, D.-S. Li, Z. J. Xu, Y. Huang, J.-M. Lu and Q. Zhang, *Small*, 2019, **15**, 1903188.
8 R. R. Kapaev, E. V. Shklyaeva, G. G. Abashev, K. J. Stevenson and P. A. Troshin, *Mendeleev Commun.*, 2022, **32**, 226.
9 O. V. Kharissova, V. A. Zhinzhilo, M. A. Chernomorova, I. E. Uflyand, I. Gómez de la Fuente and B. I. Kharisov, *Mendeleev Commun.*, 2021, **31**, 893.
10 H. Zhao, N. Deng, J. Ju, Z. Li, W. Kang and B. Cheng, *Mater. Lett.*, 2019, **236**, 101.
11 S. Gao, K. Wang, R. Wang, M. Jiang, J. Han, T. Gu, S. Cheng and K. Jiang, *J. Mater. Chem. A*, 2017, **5**, 17889.
12 J. Chai, Z. Liu, J. Ma, J. Wang, X. Liu, H. Liu, J. Zhang, G. Cui and L. Chen, *Adv. Sci.*, 2017, **4**, 1600377.
13 M. Liu, D. Zhou, Y.-B. He, Y. Fu, X. Qin, C. Miao, H. Du, B. Li, Q.-H. Yang, Z. Lin, T. S. Zhao and F. Kang, *Nano Energy*, 2016, **22**, 278.
14 F.-Q. Liu, W.-P. Wang, Y.-X. Yin, S.-F. Zhang, J.-L. Shi, L. Wang, X.-D. Zhang, Y. Zheng, J.-J. Zhou, L. Li and Y.-G. Guo, *Sci. Adv.*, 2018, **4**, eaat5383.
15 E. A. Komissarova, O. A. Kraevaya, I. S. Zhidkov, A. I. Kukharenko, N. N. Dremova, Y. V. Baskakova, A. F. Shestakov and P. A. Troshin, *Synth. Met.*, 2023, **293**, 117300.
16 H. Audi, Z. Chen, A. Charaf-Eddin, A. D’Aléo, G. Canard, D. Jacquemin and O. Siri, *Chem. Commun.*, 2014, **50**, 15140.
17 D. N. Laikov, *Chem. Phys. Lett.*, 1997, **281**, 151.

Received: 22nd June 2023; Com. 23/7201